The prenatal nicotine exposure leads to epigenetic alterations in nervous system signaling genes in the rat

Jose Antonio Muriel Muriel
Univ. Rennes, EHESP, Inserm, Irset (Institut de recherche en santé
Ouzna Dali
Univ. Rennes, EHESP, Inserm, Irset (Institut de recherche en santé
Ana Vargas Baco
Univ. Rennes, EHESP, Inserm, Irset (Institut de recherche en santé
Sergei Tevosian
University of Florida
Linda F. Hayward
University of Florida
Jasenka Zubcevic
University of Toledo
Fatima Smagulova
fatima.smagulova@inserm.fr

Univ. Rennes, EHESP, Inserm, Irset (Institut de recherche en santé

Method Article

Keywords: nicotine, testis, pituitary gland, histone marks, MeDIP, RNA-seq

Posted Date: January 25th, 2024

DOI: https://doi.org/10.21203/rs.3.rs-3888247/v1

Additional Declarations: No competing interests reported.

Version of Record: A version of this preprint was published at Epigenetics & Chromatin on May 7th, 2024.
See the published version at https://doi.org/10.1186/s13072-024-00539-5.

Abstract

Background.

Prenatal nicotine exposure (PNE) has been documented to impose numerous deleterious effects on fetal development. However, the epigenetic changes promoted by nicotine exposure on germ cell are still not well understood.

Objectives.

In this study, we focused on elucidating the impact of prenatal nicotine exposure on regulatory epigenetic mechanisms important for germ cells development.

Methods.

Sprague-Dawley rats were exposed to nicotine during pregnancy and male progeny was analyzed at 11 weeks of age. Testis morphology was analyzed using frozen testis sections and expression of germ cell markers was examined by RT-qPCR; regulatory histone modifications were assessed by Western Blot (WB). A genome-wide DNA methylation was analyzed using Methylated DNA immunoprecipitation (MeDIP)-seq. We also carried out transcriptomics analysis in pituitary gland with RNA-seq.

Results.

We show that gestational exposure to nicotine reduces germ cell numbers, perturbs meiosis, affects the expression of germ line reprogramming responsive genes and impacts the DNA methylation at nervous system genes in the testis. Besides that, PNE leads to perturbation of gene expression in the pituitary gland.

Conclusions.

Our data demonstrate that PNE leads to perturbation of male spermatogenesis and the observed effects are associated with peripheral nervous system signaling pathway changes. Alterations in the expression of genes associated with diverse roster of biological activities such as cell migration, cell adhesion and GABA signaling in the pituitary gland suggest that effects of nicotine exposure are complex and initiated via alterations in the central nervous system.

Background

Smoking, as direct or indirect nicotine consumption remains a global public concern. Despite known risks, many pregnant women are struggling to quit nicotine and continue to smoke during pregnancy. According to study published in 2018 by Lancet Global Health, the rate of smoking during pregnancy in Europe is among the highest in the world with ~ 8% of women affected [1]. Epidemiological studies provide unequivocal connection between smoking and nicotine consumption during pregnancy and health issues in children. Maternal smoking is thought to contribute to reduced fetal growth, preterm

birth, abnormal brain development, respiratory and cardiovascular issues and a higher risk of obesity, diabetes, hypertension, and other health problems later in life (e.g., [2],[3],[4]. Nicotine exposure is linked to obesity and thyroid malfunction [5],[6],[7], perturbed nervous system development [8], as well as behavioral impairment such us Attention-Deficit/Hyperactivity Disorder (ADHD) and hyperactivity [9],[10]. Importantly, nicotine exposure was documented to affect the development of male reproductive system, where it perturbs sperm motility and production of sex hormones [11].

This study is a part of a comprehensive project which was aimed to assess whether nicotine exposure (that occurs in humans during consumption of either electronic or standard cigarettes) during pregnancy in the rat affects gut microbiota, and how the alterations in microbiota composition impacts the development of nervous, cardiovascular, digestive, and reproductive systems [12]. Here, we specifically examined the epigenetic effects of nicotine on the reproductive system in male offspring.

Spermatogenesis is a process culminating in the formation of male haploid gametes. The quality of gametes is important and extends beyond simply their fitness to conceive, but also to accomplish a larger goal which is development of the healthy progeny. Thus, understanding the consequences of PNE on germ cells is important for developing policies and regulations to mitigate the risks associated with nicotine exposure in women. The first germ cell population forms during embryonic development from the somatic cells. During development, the global reprogramming of the embryo occurs where the entire genome undergoes rounds of demethylation and re-methylation in order to establish new cellular layers. Subsequent to two waves of reprogramming, a first population of germ cells emerges. Reshaping the formation of the germ line reprogramming responsive genes (GRRs) play a key role during the germ cell formation. This group of 45 genes is controlled by the ten-eleven translocation (TET) proteins; GRRs gradually lose their methylation marks while their expression increases [13],[14]. It has been shown that perturbation in demethylation at these genes results in a decreased germ cell population. A majority of GRRs are meiotic-specific genes. Thus, epigenetic state at GRRs is critical, and perturbations in their methylation and expression could lead not only to a decrease in germ cell numbers but also result in meiosis failure.

The spermatogenesis resumes after birth in testis seminiferous tubules, a network of tubular structures composed from the periphery to the lumen of less differentiated to most differentiated cellular layer. Gonocytes that range from immature to fully developed: spermatogonia, spermatocytes, round spermatids, the elongated spermatids and spermatozoa reside in the tubules. Apart from gonocytes, the Sertoli cells - large and tightly connected support cells of the testis facilitate the spermatogenesis process directly or indirectly through hormonal negative feedback systems. Star-shaped Leydig cells residing between seminiferous tubules produce sex hormones. The somatic cells of the testis assist spermatogonia to undergo replication and those tetraploid cells subsequently enter meiosis, specialized cell division to give rise to haploid gametes.

Meiosis initiation requires the coordinated action of intrinsic and extrinsic factors. An important part of meiosis is crossing over, a homologous recombination DNA exchange between a pair of homologous

chromosomes. This process is required for proper chromosome segregation before first meiotic division. It is suggested that epigenetic mechanisms are intimately involved in regulation of meiosis and spermatogenesis. Specifically, histone modifications such as γH2AX [15], H3K9me3 [16], H3K4me3 and H3K36me3 [17], ubiquitinated histones H2A [18] and H2B [19] play key roles in meiotic progression.

Here, we hypothesized that nicotine exposure could induce changes in gut microbiota composition and short-chain fatty acid synthesis that alter epigenetic landscape of the whole organism via production of acetylated groups [20].

We show that gestational exposure to nicotine reduces germ cell numbers, perturbs meiosis, affects the expression of germ line reprogramming responsive genes and impacts the DNA methylation at nervous system genes in the testis that regulate hormonal signaling. Besides that, several genes related to cell migration, cell adhesion and GABA signaling were affected in the pituitary gland of nicotine-exposed animals.

Results

The effects of nicotine exposure on the testis morphology and germ cell number

To explore the effects of maternal nicotine exposure on testis morphology of the progeny we compared hematoxylin and eosin-stained frozen testis sections in 11-week-old male animals born to the nicotine-exposed or control mothers. We examined the tubules at stage VI-VII where all cell types are known to be present to focus on homogenous cell populations between groups. We counted all the cells in a seminiferous tubule. The spermatogonia and early meiotic cells (leptotene-zygotene stage) are normally localized proximal to membrane of seminiferous tubule cells, whereas more advanced pachytene and haploid cells advance closer to the lumen (Fig. 1a-b). We found that the number of cells appears to decrease as a result of nicotine exposure by 0.7-fold (Fig. 1c). Similarly, our analysis of the seminiferous tubules thickness at stage VI-VII showed the decrease in exposed animals by 0.78-fold (Fig. 1d).

Next, we analyzed the number of germinal meiotic cells using γH2AX mark. Non-canonical phosphorylated histone variant H2AX replaces the canonical histone H2A during formation of double strand breaks (DSBs), thus allowing the chromosomes to become more condensed (reviewed in [21]). DSBs formation occurs throughout the whole genome and at each chromosome thus γH2AX is widely spread. At early stages of meiosis (leptotene-zygotene) when DSBs start to form, γH2AX appears as a very bright staining all over the nucleus. At a later stage (pachytene-diplotene), when autosomes segregate and DSBs are getting repaired, γH2AX is retained only at the sex-chromosomes as a bright spot (e.g., [22]). The γH2AX staining at cell types such as Sertoli cells as well as spermatocyte type 2, spermatogonia and spermatids is normally not strong and generally only appears as foci in case of random DNA damage. We performed the immunofluorescence assay (Fig. 2a) and calculated γH2AX positive cells as well as counted all cells in tubules. Our analysis revealed that there is 0.76-fold

decrease in γH2AX positive cells suggesting possible decrease in the meiotic cell population or delay in the initiation of the meiosis in the testis of the nicotine-exposed offspring (Fig. 2b).

To reveal which cell populations might we impacted by nicotine, we decided to analyze the expression of genes which are specifically expressed in each cell population using as a source of information a recently published dataset [23]. To this end, we extracted total RNA and performed quantitative RT-qPCR analysis. Our analysis revealed that genes that are specifically expressed in spermatogonia, *Kit* and *Lgr4*, have decreased their expression by 0.16 and 0.15- folds, respectively. In contrast the expression of *Stra8* had tendency to increase 1.5-fold (Fig. 2c). We determined that several genes that are normally expressed in spermatocytes, *Piwil1, Pttg1, H2ax* and *Rad51*, have all decreased their expression by 0.15, 0.4, 0.1 and 0.27-folds respectively. The *Kiss1* gene that is specific for Sertoli cells have increased the expression by 2.13-fold, in contrast, *Ctsl and Amhr2* genes that also are expressed in Sertoli cells have decreased their expression by 0.6 and 0.08-folds respectively (Fig. 2c). Finally, *Prm1 and Prm2*, specific for spermatid fraction have decreased and increased their expression by 0.48 and 1.2 -folds respectively (Fig. 2c).

In conclusion our morphology analysis demonstrated global decrease in germ cell population. We also observed that gene expression specific for each cell type was also perturbed suggesting that prenatal exposure to nicotine notably alters gene expression in almost all cell types of the testis.

Effects on meiosis

To further explore effects of nicotine exposure on meiosis we opted to analyze the formation of H3K9me3 marks in the nuclei. During meiosis H3K9me3 is normally localized all over the nucleus during leptotene- zygotene stages, and the H3K9me3 marks become concentrated at the nuclear periphery at pachytene-diplotene stages [24]. H3K9me3 is normally enriched at the regions of compact heterochromatin during meiosis (reviewed in [25]). During normal meiosis, H3K9me3 is observed mainly at the nuclear periphery in form of patches, and in some pathological conditions the formation of H3K9me3 patches could become perturbed. This perturbation, associated with alteration of telomere attachment and reduction of H3K9me3, leads to a loss of chromatin repression at telomeres [26]. We obtained testis spreads and immunostained the sections for H3K9me3 (Fig. 3a) followed by a quantitative analysis of mark's intensity. Our analysis showed that in PNE cells there is 1.7-fold increase in H3K9me3 staining, suggesting possible impact of nicotine and this marks on normal chromosome segregation (Fig. 3b). One of the known functional consequences for H3K9me3 increase is a decrease in TERRA transcript and reduced telomere stability [27].

Next, we sought to analyze the expression of meiotic GRR genes given their importance for normal meiosis functioning. Our analysis showed that most of tested GRR genes increased their expression including *Brdt, Dazl, Ddx4, Tdrd1* by 1.5, 1.6, 1.7, 5 -fold respectively, suggesting potential perturbation of reprograming at GRR loci due to nicotine exposure (Fig. 3c). *Hormad1* expression that is essential for meiosis [28] also had a tendency to increase by 1.2-fold (Fig. 3c).

In summary, meiosis and GRRs gene expression were perturbed in PNE male rats suggesting that PNE has a deleterious effect on the reproductive system in adults.

Analysis on protamine and regulatory histone marks

To determine the effect of nicotine on haploid cell population we analyzed the level of protamine proteins by WB (Fig. 4a). The protamines are encoded by *Prm1* and *Prm2* genes to replace histones during late stage of spermatogenesis and assist in forming a protected and compact structure of chromatin characteristic for spermatozoids. We determined that the PRM2 concentration decreased 2.4-times in exposed cells (Fig. 4b).

Next, we analyzed H3K4me3 (that marks open chromatin) and H3K9me3 that is associated with gene silencing abundant at compact heterochromatin. Our analysis showed no significant changes in the level of H3K4me3 at the global level although we cannot exclude the possibility of regional changes (Fig. 4c). On the contrary, the analysis of H3K9me3 showed a significant increase in this histone mark in nicotine-exposed samples (Fig. 4d). The results of WB of H3K9me3 are consistent with immunofluorescence analysis of H3K9me3 (Fig. 3A-B), which also showed higher level of H3K9me3 in spermatocytes suggesting global impact of nicotine exposure on H3K9me3.

In summary, the WB analysis shows that, in addition to a decrease in meiotic cell number, there is also a decrease in post-meiotic cells, which are normally enriched in PRM2 protein. The higher level of H3K9me3 during meiosis can also have an impact on compact heterochromatin and telomere functioning during meiosis.

Analysis of DNA methylation

To explore the impact of nicotine on DNA methylation we performed DNA methylation analysis using a genome-wide sequencing technique. In our study, nearly ~ 57K of CpG-rich regions were detected. We identified 366 regions that showed differential pattern of DNA methylation (FDR < 0.1) (Fig. 5a). Among differential peaks, 198 showed increased methylation and 165 regions showed decreased DNA methylation (Fig. 5b, Additional file S1). The analysis using ChIPseeker application showed that the vast majority of the differentially methylated regions (DMRs) are distally located regions. However, nearly ~ 14% of DMRs were found in introns (Fig. 5c). To determine differentially methylated genes based on the DMRs, we assigned DMRs to genes using Chipseeker. Functional annotation of differentially methylated regions (DMRs) by DAVID showed that they are enriched in genes that normally expressed in neuronal cell body (*Dmd, Tgfb1)* (Fig. 5d); they are also enriched in genes encoding transcription factors (*Foxj3, Nfact2, Rfx3, Meis3, Rbpj, Foxs1, Dmtf1, Hoxb3, Hoxa2, Tead1, E2f7, Hoxa5, Hoxb5, Creb5*), the glutamatergic synapse (*Qsec2, Dtnbp1, Cabp1, Begain, Dnm2, Olfm1, Actc1, Slitrk2, Psd2, Prkar2a, Slitrk1, Syt10, Gpc6, Adgrl3*), and GABAergic signaling factors (*Slitrk2, Slitrk1, Sst, Iqsec3, Igsf9b*) (Fig. 5e). In addition, the genes encoding estrous cycle related factors (*Trpm2, Anxa1, Cyp1b1, Pgr*) were determined to harbor DMRs.

Due to their importance for meiosis, we specifically examined DNA methylation status of 45 GRRs. We extracted the sequencing reads number of the methylated regions of GRRs and plotted them in Excel (Fig. 6a, Table S1). We found that DNA methylation marks are presents at ~ 30 genes. We observed that DNA methylation has tendency to decrease at the *Hsf5 (p = 0.1)* and is increased at *Mov10l1* gene (p = 0.008) (Fig. 6b). Notably, the decreased DNA methylation at GRRs is negatively correlates with the GRRs gene expression (Fig. 3c) suggesting a possible impact of PNE on DNA methylation at GRRs during development on GRRs gene expression in adulthood.

We also decided to determine whether there is motif enrichment in DMRs in order to reveal a possible trigger mechanism induced by PNE. To this end, we extracted sequence information of DMRs in *fasta* format and performed motif search using MEME-ChIP. Our analysis determined that two common motifs are found in many sequences. The part of the first common motif is similar to binding site of the NRF1. *Nrf1* encodes for a regulator of mitochondrial metabolism that plays a critical role in post-migrating primordial germ cells (PGC) development [29], suggesting possible role of this factor in nicotine-treated germ cells. The part of the second identified motif is similar to binding site of ETV4 (Fig. 6c). ETV4 regulates the cell proliferation [30].

To sum up, our DNA methylation analysis approach uncovered that upon nicotine exposure there is differential methylation of genes relevant to nervous system signaling and transcription factor activities. We propose that the alterations in activities in *NRF1 and ETV4* transcription factors could trigger post-migrating primordial germ cells development and proliferation.

RNA-seq analysis of pituitary gland in nicotine-exposed animals reveals effects on protein-coding genes important for cell migration, cell adhesion and GABAergic signaling.

To explore the molecular mechanisms of nicotine exposure in the neuroendocrine system, we performed transcriptomic analysis of mRNA using paired-end stranded RNA sequencing using 3 biological replicates for the *nicotine*-treated and control pituitary glands. The samples showed some variations between replicates (Fig S1a-b) due to the complexity of cellular milieu in the pituitary. However, we were able to identify 60 differentially expressed genes (FDR < 0.1) (Fig. 7a, Fig. S1c, Table S3). The majority of differentially expressed genes (DEGs) were downregulated (Fig. 7a, Fig S1d). We performed a functional annotation of the DEGs by using the gene ontology program DAVID. Our analysis showed that the strongest enrichment in DEGs was found in the genes related to *Tgfb1* signaling, regulation of cell migration, and cell adhesion among others (Fig. 7b). It is noteworthy, that *Tgfb1* beta signaling factors encoding genes (*Acta2, Col4a2)* were upregulated in pituitary gland, in contrast to *Tfgb1* DNA methylation decrease in the testis in exposed animal, suggesting thereby a possible link between brain and testis *Tfgb1* signaling pathways.

Since we observed some alteration in DNA methylation of GABAergic signaling genes, we decided to closer look at these genes in our RNA-seq data. To this end, we determined the genes that are combined by gene ontology term “GABAergic synapse” using AMIGO database (https://amigo.geneontology.org/amigo). 136 genes were related to this term, with 121 out of them were

expressed in the rat pituitary gland. We determined that *Erbb4* and *Slc6a6* were significantly upregulated upon nicotine exposure and three genes (*Slc6a11, Slc32a1, Slc6a6*) showed tendency to increase. Six genes (*Gabra4, Gabrg2, Epha3, Gabra3, Gap43, Adra2a*) showed tendency to decrease (Fig. 7C). These altered genes encode for proteins that are combined in network with central players GABRA2, GABRA3 and GABRA4, GABRG2 (Fig. 7d).

In summary, RNA-seq analysis showed that genes related to *Tgfb1* signaling, cell migration, cell adhesion and GABAergic signaling were differential between control and nicotine groups, suggesting that prenatal exposure to nicotine affects the neuroendocrine system as well.

Discussion

Here we examined testes of male offspring from rats exposed to nicotine during pregnancy. Our analysis showed that testis morphology in PNE animals was changed. Specifically, we observed that total number of germ cells per tubule has decreased. This could possibly be explained through the effects of nicotine exposure on GRR genes as they are known to impact the formation of the entire population of germ cells [13]. We conclude that nicotine exposure has the potential to globally affect meiosis. We also observed gene expression changes in germ line (spermatogonia and spermatocytes) as well as in somatic (Sertoli) cells suggesting that meiosis could be perturbed by nicotine through action on both somatic and germ cell compartment. For example, decrease in *Rad51* (recombinase) and *Hormad1* (recombination and cell cycle regulation) genes' expression could lead to alterations in homologous recombination.

While we cannot exclude the possibility that nicotine directly induces the changes we observed in the testis, we believe the indirect effect to be more plausible. Changes in DNA methylation of genes in the nervous system could affect the production of sexual hormones and the observed effects could be due to perturbation of nervous system signaling. Specifically, we observed alterations in the expression of the molecular components for glutamatergic system (Fig. 5e). Indeed, glutamate transporters (VGLUTs) are expressed in the testis, for example, VGLUT2 is expressed and localized in the outer acrosomal membrane of spermatids, suggesting that glutamatergic system has a function in the testis [31]. In this respect, GABA, a major neurotransmitter in the central nervous system, also acts as a signaling molecule in endocrine tissues such as pituitary and testis [32]; reviewed in [33]. Testicular Leydig cells are both producers and targets for GABA signaling [34]. These cells express GABA(A) receptor subunits, and in the murine Leydig cell line TM3 pharmacological activation leads to their increased proliferation. TM3 cells not only express GABA (A) receptor subunits, but also bind the GABA agonist; GABA or GABA(A) agonist isoguvacine treatment led to changes in the expression of transcription factors and cell cycle-associated genes [35], [36], [37].

Importantly, we found the increase in the expression of *Erbb4* gene in pituitary gland of nicotine-exposed rats. Notably, ERBB4 have been previously linked to nicotine addiction where genome-wide association (GWA) and candidate gene studies for smoking behavior and nicotine dependence revealed that ERBB4

is a strong candidate for nicotine dependence, as several mutations were identified in addicted persons [38]. On the other hand, it has been reported that nicotine controls synaptic plasticity through NRG3/ErbB4-dependent regulation of GABAergic inhibition [39]. A significant increase in *Erbb4* and *Nrg3* expression were reported following chronic nicotine exposure and withdrawal in mice [40]. Thus, it is possible that nicotine consumption increases the expression of *Erbb4* that in turn have the inhibitory effects on GABAergic signaling. Small decrease in GABAergic receptors genes in our study is in line with this hypothesis.

We also observed a decrease in DNA methylation of GABAergic signaling genes such as *Iqsec3, Igsf9b and Sst* in the testis. Notably, *Sst* gene encodes for somatostatin protein. In testis SST receptor is expressed in Leydig cells [41], and somatostatin is known to inhibit proliferation of male germ cells [42]. Thus, we suggest that decreased level of methylation of *Sst* could affect its expression and impact germ cell proliferation. We also suggest that, similar to brain tissue, the GABAergic effects in the testis could be additionally mediated via *Erbb4*, as *Erbb4* is expressed in Sertoli cells and affects Leydig cells through paracrine mechanism [43]. Further work is required to confirm this statement.

Finally, gene expression changes in Leydig cells could perturb hormonal signaling. For example, we detected a decrease in DNA methylation of progesterone receptor gene. Testicular progesterone has been regarded as a by-product of steroidogenesis, which is not converted into testosterone. Serum 17-OHP appears to be a reliable serum marker for intratesticular testosterone levels and could potentially be used as a readout to titrate or change medications that alter intratesticular testosterone. Similar, based on this data we can assume that there is likely to be a perturbation in testosterone concentration [44].

Western blots and DNA methylation analysis indicate that nicotine exposure results in the overall repression of studied genes, led by reduction of open chromatin complexes and increase in repression H3K9me3 histone mark. As DNA methylation and histone marks are functionally linked, it is conceivable that alterations in either DNA methylation or histone marks could induce a cascade of events leading to a global change in chromatin architecture and gene expression.

Conclusion

In summary, we determined that PNE affects the expression of a wide range of genes related to transcription and nervous system function. We suggest that alterations in gene expression and epigenetic control perturb germ cell proliferation and normal testis development. This study revealed several biomarker genes (*Erbb4, Tgfb1, Nrf1, Etv4*) that could be used for the analysis of nicotine effects in human studies.

Materials and methods

Experimental design

Outbred Sprague-Dawley pregnant rats were treated either with vehicle (control) or a low nicotine dose. After the treatment, the male offspring of these animals was euthanized at 11 weeks of age and testes were dissected and examined. Specifically, we analyzed testis morphology, profiled gene expression and meiosis as well as documented histone status by Western blot. We also performed genome-wide analysis of DNA methylation in the testis (MeDIP-seq) and completed bioinformatic analysis to identify signaling pathways affected by gestational exposure to nicotine. Finally, we performed transcriptomic analysis of pituitary gland gene expression using stranded paired RNA-sequencing to identify new biomarkers of exposure that could be useful in human studies.

Animal treatment

Specific pathogen-free male and female Sprague Dawley rats were purchased from Envigo (USA). Females were purchased at 8 weeks of age and were allowed 1 week to acclimate. At 9 weeks of age, females were randomly assigned to one of 4 treatment groups. Two groups of females were mated, and two groups of females remained virgins. Mating included placing a single female overnight with a male and examination on the following morning for the presence of sperm via vaginal swabs. If sperm was present, the dam was weighed and placed in a separate cage, and this period was marked as gestational day (GD) 0. If no sperm was detected, the pair remained together, and the female was examined daily until pregnancy and GD0 were confirmed. Using a sterile technique, a 28-day osmotic mini-pump (2ML4-ALZET, Durect Corp., Cupertino, CA, USA) filled with either sterile saline (control; CON) or a nicotine tartrate (6 mg/kg; NIC), dissolved in sterile saline was placed subcutaneously between the scapulae, as described before [45, 46]. On GD19, or 13 days following pump surgery, dams were allowed to give birth.

Male progeny from both control and nicotine dams was sacrificed at 11 weeks of age. Animals were anesthetized at a surgical plane with isoflurane (2.5% in 100% oxygen), and blood was collected from the aorta for detection of circulating plasma leptin and SCFA content. Following this, all animals were given an overdose of sodium pentobarbital (> 200 mg/kg). Several organs, including pituitary and testes in the males, were collected and preserved in liquid nitrogen.

RNA extraction, quantification & cDNA synthesis and RT-QPCR

Testicles stored at − 80 ºC from the control and treatment group were used for RNA extraction. The extraction was performed using RNeasy Plus Mini Kit 250 (Qiagen, 74134). Approximately 30 mg of each testis was used (6 biological replicates). Testicles samples were lysed and homogenized using TissueLyser (Qiagen). Once homogenized, the RNA extraction protocol was followed. Purified RNA was then eluted in 50 µL of RNase-free water. RT was performed using 1 µg of total RNA with iScript (Bio-Rad, 1708891) adhering to the Minimum Information for Publication of Quantitative Real-Time PCR Experiments (MIQE) guidelines (Bustin et al. 2009). We used *Rpl37a* as a housekeeping gene because it showed no variation between replicates based on RNA-seq data. The data are presented as the fold change relative to the control ± SD. Primers for this study were selected using the Primer-Blast program

from ncbi.nih.gov, and most of them included exon-to-exon junctions; the primers are listed in Table S2. A nonparametric Mann–Whitney test was used for evaluating statistical significance.

MeDIP, library preparation and MeDIP-seq analysis

DNA was extracted from 6 biological replicates using DNA Easy Blood and Tissue Kit (Qiagen, 69506) according to instructions provided by the manufacturer. DNA concentration was measured by fluorescent method using fluorescent reader (Promega). 10 µgs of DNA was used for MeDIP using methylated DNA Enrichment Kit (NEB, #E2600S). DNA was diluted and sonicated in Qsonica 700 sonicator (Q700-110, Newtown, Connecticut, USA) supplied with cup horn 431C2 using following conditions: 20 s pulse on, 20 sec pulses off, total sonication time is 8 min; these parameters allow to obtain ~ 300 bp DNA fragments. After that, methylated DNA was extracted with A/G beads and the concentration of methylated DNA was again determined by fluorescence. Equal amounts of methylated DNA and input (7 ng) were taken for library preparation. Sequencing libraries were prepared using the NEBNext Ultra DNA Library Prep Kit for Illumina (E7645S; NEB). Sequencing was performed on an Illumina HiSeq4000 sequencer using a paired-end 50-base read in multiplexed mode. An average of 44 million sequencing reads per sample were processed. The exact number of reads per sample is provided in Table S3. The reads were mapped to the reference genome rn7 v2.5.0 using Bowtie (Langmead et al. 2009). The numbers of mapped reads were normalized by a scale factor to adjust the total number of reads using Samtools program. From the aligned reads, DNA methylated peaks were identified using six biological replicates and the corresponding input by the MACS2 (2.2.7.1) algorithm [47]; the following parameters were applied: a shift-size window of 73 bp, no model, and a q-value threshold < 0.05. For comparison of the control datasets of the nicotine-exposed and control samples, differential peaks were identified using counting reads at each peak using bedtools MultiCovBed (Version 2.30.0) [48]. Statistical significance was calculated using DeSeq2 (v2.11.40.8) [49] with filtering peaks with low counts. We performed functional annotation of the differential peaks using the web-based tool ChIPseeker v1.28.3 [50] (using default parameters). For the visualization of ChIP-seq tracks, each .bam file was converted to BedGraph tracks by using Genome Coverage 2.30.0. IGV was used to visualize the tracks. Functional annotation of genes localized in differentially methylated regions was performed with the DAVID program using “Biological process”, “Molecular function”, “Cellular Component” [51].

RNA sequencing and data processing.

We used three biological replicates from the control group and three for nicotine group of rats. RNA was extracted using RNeasy kit as described above. RNA was additionally treated with DNAse I (QIAGEN, 79254). One microgram of total RNA was used for a strand-specific library preparation protocol using NEBNext Ultra II Directional RNA Library according to the protocol provided by the manufacturer. Quality control and genome-wide sequencing were performed at the GenomEast platform at the Institute of Genetic, Molecular and Cellular Biology (IGBMC), Strasbourg, France. The sequencing was performed in massive parallel sequencing using paired-end mode, and the size of the sequencing tag was 100 bp. Reads in FASTQ format were processed for quality control using the FastQC tool

(http://www.bioinformatics.babraham.ac.uk/projects/fastqc/). An average of 61 million sequencing reads per sample were processed. The exact number of reads per sample is provided in Table S4. The reads were mapped to the reference genome [Rattus Norvegicus rn7 sequence] using the HISAT2 [52] alignment program with default parameters, and the alignment files were generated as BAM files. These files were used as the input for FeatureCounts to calculate the gene abundance using the gene annotation file ncbiRefSeq.gtf.gz from UCSC. Differential gene expression was assessed using the package DESeq2 (2.11.40.7) with the option of filtering genes with low counts. Functional annotation of differentially expressed genes (DEGs) was performed with the DAVID [51] program using “Biological process”, “Cellular component” or “Molecular function” ontologies as background set the genes which are normally expressed in adult pituitary gland.

Histone extraction

The protein extraction was conducted using a Histone Extraction Kit (Abcam, ab113476) according to the protocol provided by the manufacturer. Testicles stored at − 80°C were used for histone extraction. Briefly, samples were homogenized with a TissueLyser (Qiagen) and cell extracts were pelleted via centrifugation. After some centrifugations and resuspending, the supernatant with histone extracts was collected and 0.3 volumes of Balance-DTT Buffer were added. Histone protein concentrations were quantified using Bio-Rad iMark™ microplate reader reading at 660 nm using Bradford solution.

Western blotting

Western blots were performed for the control and nicotine exposed samples using the following antibodies: rabbit anti-H3K4me3 (1:10000, Millipore 07-473), rabbit anti-H3K9me3 (1:10000 Abcam, ab8898), goat anti-protamine 2 (1:200, Santa Cruz Biotechnology, sc-23104). Extracted histones (as described above) were used for Western blotting. Concentrations of each protein sample obtained from OD readings, were used to determine an exact volume containing 10 µg of histone protein for each sample. Aliquots of 10 µL containing 25 mM RIPA Buffer, Laemmli 3X buffer, and sample volumes containing 10 µg of histone proteins were denatured at 95 ºC for 5 min and run on a 4–20% gradient acrylamide gel Mini-PROTEAN TGX Stain-Free Gels (BioRad). Proteins were transferred onto Polyvinylidene difluoride (PVDF) membranes Trans-Blot Turbo Transfer Pack (BioRad) using a Trans-Blot® Turbo™ Transfer System (BioRad). Ponceau Red staining was conducted to determine the relative abundance of total histone proteins. Images were collected using Molecular Imager ChemiDoc™ XRS + with Image Lab™ Software (BioRad). Blocking was conducted using a 5% milk in 1X TBS Tween 0.05%. The primary antibodies were diluted to different ratios in 10 mL of the blocking solution, introduced to each membrane in small plastic boxes and incubated overnight at 4ºC. After three 5-min washes with 1X PBS Tween 0,05%, each membrane was incubated for 1 h in 10 mL of the blocking solution containing the corresponding secondary antibodies (1:10000 for anti-rabbit and 1:5000 for anti-mouse). After another three 5-min washes with 1X PBS Tween 0,05% the blots were exposed ECL Prime Western Blotting Detection Reagent (RPN2232; Amersham). Specific protein expression for each antibody was documented using a molecular imager. Ponceau Red staining was conducted to determine the relative abundance of total histone proteins. The intensity of total histone abundances were used to normalize

the occupancy of each specific epigenetic marker. Intensity of the bands were measured in ImageJ-Fiji software. Western blotting signals were presented as averaged normalized values relative to Ponceau Red.

RT-qPCR

Reverse transcription of 1000ngs RNA was performed with the iScript cDNA synthesis (BioRad). Reactions were loaded into 384-Well PCR plates (BioRad) along with iTaq Universal SYBR®Green Supermix (BioRad), primers (Eurogentec), and MilliQ water. Each well contained 5µL of SYBR®Green Supermix, 0,05µL of each primer pair of primers (100uM stock solution), 0,9 µL of H_2O, and 4µL of DNA. The amplification was carried out in CFX Opus384 (BioRad) with the following protocol: initial denaturation (98°C- 30sec) followed by 40-amplification cycle program (98°C-15sec and 65°C-60sec). Normalized values were calculated with CFX Manager program using *Rpl37a* as a reference housekeeping gene.

Immunostaining of rat seminiferous tubules

Samples of testicles were taken and placed in OCT compound prior to cryostat sectioning and kept in -80^{O}C until use. The samples were cut in sections with the microtome at 7 µm and mounted on Matsunami TOMO® hydrophilic adhesion slides. The slides were left to dry at room temperature for about 30 minutes. Once dried, 4% buffered paraformaldehyde was added and the slides were incubated for 8 mins. Slides were quenched with 0.1M Glycine in PBS and washed twice with PBS to remove residual glycine. A blocking solution (4% BSA in PBS) was added for 30 mins at RT. Once blocking phase was finished, slides were rinsed with PBS three times and the first antibody solution was added diluted in DAKO: rabbit anti-γH_2AX (1:500, TREVIGEN, 4418-APC-100). Antibodies were incubated overnight at 4ºC. After incubation and rinsing, secondary antibodies also diluted in DAKO at a dilution of 1:500 (Invitrogen AlexaFluor®) were added and incubated at RT for 1 hour. After three washes, the Vectorshield solution containing DAPI staining was added to each slide. The counting was performed using ImageJ application. We calculated ratio of γH2AX-positive cells to a total cell number in a seminiferous tubule.

Preparation and immunostaining of structurally preserved nuclei.

Structurally preserved nuclei (SPN) for three-dimensional analysis were prepared by cutting testis tissues in DMEM medium (Life Technologies, GIBCO) with 0.5% protease inhibitor. The cell suspensions were mixed with equal amounts of 3.7% (vol/vol) paraformaldehyde and 0.1 M sucrose and spread on glass slides. The slides were air-dried and kept at -80°C. The slides were then washed several times with PBS and 2 min with 0.1M glycine in PBS to remove the traces of paraformaldehyde before use. Slides were permeabilized during a 30 min incubation in PBS/0.5%Triton at RT, washed with PBS, and blocked for 30 min in a solution containing 0.1% (v/v) donkey serum, 0.03% (w/v) BSA, and 0.005% (v/v) Triton X-100 in PBS. SPN were immunostained with rabbit H3K9me3 (Abcam, ab8898, 1:500) and mouse monoclonal SYCP3 (1:200, Santa Cruz, SC-33195) antibodies at 4°C overnight followed by several washes and incubation with Fluorescent Alexa antibodies. Z-stacks were acquired with 500 nm steps. 15 planes were

taken for each individual channel, DAPI (Blue, 350nm), SYCP3 (Red, 594nm) and H3K9me3 (Green, 488nm) using Zen Pro (version 2.3). All images for control and exposed samples were taken with fixed exposure times. Deconvolution was performed using the “Fast Iterative” algorithm provided by Zen Pro. The sum intensity images were generated for each z-stack and the resulting images were analyzed in ImageJ v1.52n. We used the lasso tool for nucleus contouring, and the integrated density immunofluorescence for each nucleus was calculated. The background area was subtracted from each image. We analyzed four independent biological replicates for control and treated group. The data were plotted in Excel and presented as corrected total cell fluorescence (CTCF) of normalized fluorescence for nucleus +/-SD, **p < 0.01, Mann-Whitney test.

Hematoxylin-eosin staining

The slides for this procedure were prepared and analyzed in the same way as presented for immunostaining. For morphology analysis, the testes from control and nicotine-treated groups were fixed in 4% (w/v) PFA solution for 8 min and washed. The sections were stained with Hematoxylin and Eosin (H&E) as per the standard protocol. The images were taken with NanoZoomer and quantitative analysis was performed using ImageJ. Images with tubules showing the presence of all cell types including the presence of elongated spermatids (stage VI or VII) were used for cell counts using ImageJ application. Cells were enumerated and divided by the total area of the tubule. We counted cells in a minimum of 10 tubules using 4 biological replicates. Statistical significance was assessed with Mann-Whitney test. For the cell thickness size analysis, we measured the thickness from the bottom of seminiferous tubule to the end of cell layers. We measured diameters in (stage VI or VII) tubules found in each section. Statistical significance was assessed with a nonparametric Mann-Whitney test.

Statistical analyses

We used the minimum number of animals required to obtain a statistically significant set of data according to the requirements of the USA ethics committee. The number of animals used is specified for each experimental procedure. A nonparametric Wilcoxon-Mann—Whitney for RT-qPCR experiments, immunofluorescence, germ cells quantifications and WB assay was used.

List of abbreviations

17-OHP	17-hydroxyprogesterone
Acrv1	acrosomal vesicle protein 1
Acta2	actin alpha 2, smooth muscle
Actc1	actin, alpha, cardiac muscle 1
Adgrl3	adhesion G protein-coupled receptor L3
ADHD	Attention-Deficit/Hyperactivity Disorder
Adra2a	adrenoceptor alpha 2A
Amhr2	anti-Mullerian hormone receptor type 2
Anxa1	annexin A1
Begain	brain-enriched guanylate kinase-associated
Brdt	bromodomain testis associated
Cabp1	calcium binding protein 1
Col4a2	collagen type IV alpha 2 chain
CrebB5	CAMP Responsive Element Binding Protein 5
Ctsl	cathepsin L
Cyp1b1	cytochrome P450, family 1, subfamily b, polypeptide 1
Dazl	deleted in azoospermia-like
Ddx4	DEAD-box helicase 4
Dmd	dystrophin
Dmtf1	cyclin D binding myb-like transcription factor 1
Dnm2	dynamin 2
Dtnbp1	dystrobrevin binding protein 1
E2f7	E2F transcription factor 7
Epha3	Eph receptor A3
Erbb4	erb-b2 receptor tyrosine kinase 4
ETV4	ETS variant transcription factor 4
Foxj3	forkhead box J3
Foxs1	forkhead box S1
Gabra3	gamma-aminobutyric acid type A receptor subunit alpha 3

Gabra4	gamma-aminobutyric acid type A receptor subunit alpha 4
Gabrg2	gamma-aminobutyric acid type A receptor subunit gamma 2
Gap43	growth associated protein 43
GD	gestational day
Gpc6	glypican 6
GRRs	germ line reprogramming responsive genes
H2ax	H2A.X variant histone
Hormad1	HORMA domain containing 1
Hoxa2	homeobox A2
Hoxa5	homeobox protein Hox-A5
Hoxb3	homeo box B3
Hoxb5	homeo box B5
Hsf1	heat shock transcription factor 1
Igsf9b	Immunoglobulin Superfamily Member 9B
Iqsec2	IQ motif and Sec7 domain ArfGEF 2
Iqsec3	IQ motif and Sec7 domain ArfGEF 3
Kiss1	KiSS-1 metastasis-suppressor
Kit	KIT proto-oncogene receptor tyrosine kinase
Lgr4	leucine-rich repeat-containing G protein-coupled receptor 4
MeDIP	Methylated DNA immunoprecipitation
Meis3	Meis homeobox 3
Mov10l1	Mov10 like RISC complex RNA helicase 1
Nfact2	Nuclear Factor Of Activated T Cells 2
Nrf1	nuclear respiratory factor 1
Olfm1	olfactomedin 1
Pgr	progesterone receptor
Piwil1	piwi-like RNA-mediated gene silencing 1
PNE	Prenatal nicotine exposure
Prkar2a	protein kinase cAMP-dependent type II regulatory subunit alpha

Prm1	protamine 1
Prm2	protamine 2
Psd2	pleckstrin and Sec7 domain containing 2
Pttg1	PTTG1 regulator of sister chromatid separation, securin
Rad51	RAD51 recombinase
Rbpj	recombination signal binding protein for immunoglobulin kappa J region
Rfx3	regulatory factor X3
Slc32a1	solute carrier family 32 member 1
Slc6a6	solute carrier family 6 member 6
Slitrk1	SLIT and NTRK-like family, member 1
Slitrk2	SLIT and NTRK-like family, member 2
Spaca1	sperm acrosome associated 1
Sst	somatostatin
Stra8	stimulated by retinoic acid 8
Syt10	synaptotagmin 10
Tdrd1	tudor domain containing 1
Tead1	TEA domain transcription factor 1
TERRA	Telomeric Repeat-containing RNA
TET	ten-eleven translocation
Tgfb1	transforming growth factor, beta 1
Trpm2	transient receptor potential cation channel, subfamily M, member 2

Declarations

Ethics approval

All animal procedures were approved by the University of Florida Institutional Animal Care and Use Committee (IACUC) prior to the start of the study (#20180188, Tevosian, SG Associate Professor, The PI).

Availability of data and materials

The datasets generated and analyzed during the current study are available in the NCBI Gene Expression Omnibus (GEO; https://www.ncbi.nlm.nih.gov/geo/) under the accession number GSE253596.

Competing interests

No competing interests to be declared.

Funding

This research was funded in part by the Florida Department of Health James and Esther King Biomedical Research Program (JZ, ST, and LFH).

Author Contributions

OD, JAMM, AVB, FS, JZ, ST Methodology. **LFH, ST, FS** Conceptualization, Investigation, Supervision, Methodology, Writing-original draft preparation.

Acknowledgments

Sequencing was performed by the GenomEast platform, a member of the “France Génomique” consortium (ANR-10-INBS-0009). We would also like to thank the Galaxy platform for bioinformatic support [53]. We would also like to thank the H2P2 platform (UMS Biosit Inserm UMS 018, CNRS UMS3480) for assistance with the preparation and analysis of frozen testis sections. We are grateful to Gennady Margolin for suggestions for the analysis in manuscript.

References

1. Lange S, Probst C, Rehm J, Popova S. National, regional, and global prevalence of smoking during pregnancy in the general population: a systematic review and meta-analysis. Lancet Glob Health. 2018;6:e769–76.
2. Madley-Dowd P, Kalkbrenner AE, Heuvelman H, Heron J, Zammit S, Rai D, et al. Maternal smoking during pregnancy and offspring intellectual disability: sibling analysis in an intergenerational Danish cohort. Psychol Med. 2022;52:1847–56.
3. Di H-K, Gan Y, Lu K, Wang C, Zhu Y, Meng X, et al. Maternal smoking status during pregnancy and low birth weight in offspring: systematic review and meta-analysis of 55 cohort studies published from 1986 to 2020. World J Pediatr. 2022;18:176–85.
4. Sukjamnong S, Chan YL, Zakarya R, Saad S, Sharma P, Santiyanont R, et al. Effect of long-term maternal smoking on the offspring’s lung health. Am J Physiol Lung Cell Mol Physiol. 2017;313:L416–23.
5. Ma N, Nicholson CJ, Wong M, Holloway AC, Hardy DB. Fetal and neonatal exposure to nicotine leads to augmented hepatic and circulating triglycerides in adult male offspring due to increased expression of fatty acid synthase. Toxicol Appl Pharmacol. 2014;275:1–11.

6. Peixoto TC, Gaspar de Moura E, Quitete FT, Simino LA, Torsoni AS, Torsoni MA, et al. Early life nicotine exposure alters mRNA and microRNA expressions related to thyroid function and lipid metabolism in liver and BAT of adult wistar rats. Mol Cell Endocrinol. 2021;523:111141.
7. Smart SJ, Nikaj AN, Yu L, Li H, Yan F, Zhang J. Association between maternal smoking during pregnancy and offspring overweight in U.S.-born children. Pediatr Obes. 2021;16:e12717.
8. Silva JP, Lambert G, van Booven D, Wahlestedt C. Epigenomic and metabolic responses of hypothalamic POMC neurons to gestational nicotine exposure in adult offspring. Genome Med. 2016;8:93.
9. McCarthy DM, Morgan TJ, Lowe SE, Williamson MJ, Spencer TJ, Biederman J, et al. Nicotine exposure of male mice produces behavioral impairment in multiple generations of descendants. PLoS Biol. 2018;16:e2006497.
10. Zhang M, Zhang D, Dai J, Cao Y, Xu W, He G, et al. Paternal nicotine exposure induces hyperactivity in next-generation via down-regulating the expression of DAT. Toxicology. 2020;431:152367.
11. Zeid D, Gould TJ. Impact of nicotine, alcohol, and cocaine exposure on germline integrity and epigenome. Neuropharmacology. 2020;173:108127.
12. Zubcevic J, Watkins J, Lin C, Bautista B, Hatch HM, Tevosian SG, et al. Nicotine Exposure during Rodent Pregnancy Alters the Composition of Maternal Gut Microbiota and Abundance of Maternal and Amniotic Short Chain Fatty Acids. Metabolites. 2022;12:735.
13. Hill PWS, Leitch HG, Requena CE, Sun Z, Amouroux R, Roman-Trufero M, et al. Epigenetic reprogramming enables the transition from primordial germ cell to gonocyte. Nature. 2018;555:392–6.
14. Wrighton KH. Reprogramming: Methylation patterns in primordial germ cells. Nat Rev Mol Cell Biol. 2018;19:278–9.
15. Mahadevaiah SK, Turner JM, Baudat F, Rogakou EP, de Boer P, Blanco-Rodríguez J, et al. Recombinational DNA double-strand breaks in mice precede synapsis. Nat Genet. 2001;27:271–6.
16. Takada Y, Naruse C, Costa Y, Shirakawa T, Tachibana M, Sharif J, et al. HP1γ links histone methylation marks to meiotic synapsis in mice. Development. 2011;138:4207–17.
17. Buard J, Barthès P, Grey C, de Massy B. Distinct histone modifications define initiation and repair of meiotic recombination in the mouse. EMBO J. 2009;28:2616–24.
18. Baarends WM, Wassenaar E, van der Laan R, Hoogerbrugge J, Sleddens-Linkels E, Hoeijmakers JHJ, et al. Silencing of unpaired chromatin and histone H2A ubiquitination in mammalian meiosis. Mol Cell Biol. 2005;25:1041–53.
19. Xu Z, Song Z, Li G, Tu H, Liu W, Liu Y, et al. H2B ubiquitination regulates meiotic recombination by promoting chromatin relaxation. Nucleic Acids Res. 2016;44:9681–97.
20. Nohesara S, Abdolmaleky HM, Thiagalingam S. Epigenetic Aberrations in Major Psychiatric Diseases Related to Diet and Gut Microbiome Alterations. Genes (Basel). 2023;14:1506.

21. Turinetto V, Giachino C. Multiple facets of histone variant H2AX: a DNA double-strand-break marker with several biological functions. Nucleic Acids Res. 2015;43:2489–98.
22. Alavattam KG, Maezawa S, Andreassen PR, Namekawa SH. Meiotic sex chromosome inactivation and the XY body: a phase separation hypothesis. Cell Mol Life Sci. 2021;79:18.
23. Green CD, Ma Q, Manske GL, Shami AN, Zheng X, Marini S, et al. A Comprehensive Roadmap of Murine Spermatogenesis Defined by Single-Cell RNA-Seq. Dev Cell. 2018;46:651-667.e10.
24. Liu Y, Zhang Y, Yin J, Gao Y, Li Y, Bai D, et al. Distinct H3K9me3 and DNA methylation modifications during mouse spermatogenesis. J Biol Chem. 2019;294:18714–25.
25. Levinsky AJ, McEdwards G, Sethna N, Currie MA. Targets of histone H3 lysine 9 methyltransferases. Front Cell Dev Biol. 2022;10:1026406.
26. Udugama M, M Chang FT, Chan FL, Tang MC, Pickett HA, R McGhie JD, et al. Histone variant H3.3 provides the heterochromatic H3 lysine 9 tri-methylation mark at telomeres. Nucleic Acids Res. 2015;43:10227–37.
27. Bettin N, Oss Pegorar C, Cusanelli E. The Emerging Roles of TERRA in Telomere Maintenance and Genome Stability. Cells. 2019;8:246.
28. Shin Y-H, Choi Y, Erdin SU, Yatsenko SA, Kloc M, Yang F, et al. Hormad1 mutation disrupts synaptonemal complex formation, recombination, and chromosome segregation in mammalian meiosis. PLoS Genet. 2010;6:e1001190.
29. Wang P, Su J, Wang J, Xie Y, Chen W, Zhong J, et al. NRF1 promotes primordial germ cell development, proliferation and survival. Cell Prolif. 2024;57:e13533.
30. Cosi I, Pellecchia A, De Lorenzo E, Torre E, Sica M, Nesi G, et al. ETV4 promotes late development of prostatic intraepithelial neoplasia and cell proliferation through direct and p53-mediated downregulation of p21. J Hematol Oncol. 2020;13:112.
31. Hayashi M, Morimoto R, Yamamoto A, Moriyama Y. Expression and localization of vesicular glutamate transporters in pancreatic islets, upper gastrointestinal tract, and testis. J Histochem Cytochem. 2003;51:1375–90.
32. Metzeler K, Agoston A, Gratzl M. An Intrinsic gamma-aminobutyric acid (GABA)ergic system in the adrenal cortex: findings from human and rat adrenal glands and the NCI-H295R cell line. Endocrinology. 2004;145:2402–11.
33. Gladkevich A, Korf J, Hakobyan VP, Melkonyan KV. The peripheral GABAergic system as a target in endocrine disorders. Auton Neurosci. 2006;124:1–8.
34. Geigerseder C, Doepner R, Thalhammer A, Frungieri MB, Gamel-Didelon K, Calandra RS, et al. Evidence for a GABAergic system in rodent and human testis: local GABA production and GABA receptors. Neuroendocrinology. 2003;77:314–23.
35. Doepner RFG, Geigerseder C, Frungieri MB, Gonzalez-Calvar SI, Calandra RS, Raemsch R, et al. Insights into GABA receptor signalling in TM3 Leydig cells. Neuroendocrinology. 2005;81:381–90.

36. Eliasen JN, Krall J, Frølund B, Kohlmeier KA. Sex-specific alterations in GABA receptor-mediated responses in laterodorsal tegmentum are associated with prenatal exposure to nicotine. Dev Neurobiol. 2020;80:178–99.
37. Geigerseder C, Doepner RFG, Thalhammer A, Krieger A, Mayerhofer A. Stimulation of TM3 Leydig cell proliferation via GABA(A) receptors: a new role for testicular GABA. Reprod Biol Endocrinol. 2004;2:13.
38. Loukola A, Wedenoja J, Keskitalo-Vuokko K, Broms U, Korhonen T, Ripatti S, et al. Genome-wide association study on detailed profiles of smoking behavior and nicotine dependence in a twin sample. Mol Psychiatry. 2014;19:615–24.
39. Zhou L, Fisher ML, Cole RD, Gould TJ, Parikh V, Ortinski PI, et al. Neuregulin 3 Signaling Mediates Nicotine-Dependent Synaptic Plasticity in the Orbitofrontal Cortex and Cognition. Neuropsychopharmacology. 2018;43:1343–54.
40. Loukola A, Wedenoja J, Keskitalo-Vuokko K, Broms U, Korhonen T, Ripatti S, et al. Genome-wide association study on detailed profiles of smoking behavior and nicotine dependence in a twin sample. Mol Psychiatry. 2014;19:615–24.
41. Fombonne J, Csaba Z, von Boxberg Y, Valayer A, Rey C, Benahmed M, et al. Expression of somatostatin receptor type-2 (sst2A) in immature porcine Leydig cells and a possible role in the local control of testosterone secretion. Reprod Biol Endocrinol. 2003;1:19.
42. Baou N, Bouras M, Droz JP, Benahmed M, Krantic S. Evidence for a selective loss of somatostatin receptor subtype expression in male germ cell tumors of seminoma type. Carcinogenesis. 2000;21:805–10.
43. Naillat F, Veikkolainen V, Miinalainen I, Sipilä P, Poutanen M, Elenius K, et al. ErbB4, a receptor tyrosine kinase, coordinates organization of the seminiferous tubules in the developing testis. Mol Endocrinol. 2014;28:1534–46.
44. Lima TFN, Patel P, Blachman-Braun R, Madhusoodanan V, Ramasamy R. Serum 17-Hydroxyprogesterone is a Potential Biomarker for Evaluating Intratesticular Testosterone. J Urol. 2020;204:551–6.
45. Chang G-Q, Karatayev O, Leibowitz SF. Prenatal exposure to nicotine stimulates neurogenesis of orexigenic peptide-expressing neurons in hypothalamus and amygdala. J Neurosci. 2013;33:13600–11.
46. Boychuk CR, Hayward LF. Prenatal nicotine exposure alters postnatal cardiorespiratory integration in young male but not female rats. Exp Neurol. 2011;232:212–21.
47. Zhang Y, Liu T, Meyer CA, Eeckhoute J, Johnson DS, Bernstein BE, et al. Model-based analysis of ChIP-Seq (MACS). Genome Biol. 2008;9:R137.
48. Quinlan AR, Hall IM. BEDTools: a flexible suite of utilities for comparing genomic features. Bioinformatics. 2010;26:841–2.
49. Love MI, Huber W, Anders S. Moderated estimation of fold change and dispersion for RNA-seq data with DESeq2. Genome Biol. 2014;15:550.

50. Yu G, Wang L-G, He Q-Y. ChIPseeker: an R/Bioconductor package for ChIP peak annotation, comparison and visualization. Bioinformatics. 2015;31:2382–3.
51. Sherman BT, Hao M, Qiu J, Jiao X, Baseler MW, Lane HC, et al. DAVID: a web server for functional enrichment analysis and functional annotation of gene lists (2021 update). Nucleic Acids Res. 2022;50:W216–21.
52. Kim D, Paggi JM, Park C, Bennett C, Salzberg SL. Graph-based genome alignment and genotyping with HISAT2 and HISAT-genotype. Nat Biotechnol. 2019;37:907–15.
53. Galaxy Community. The Galaxy platform for accessible, reproducible and collaborative biomedical analyses: 2022 update. Nucleic Acids Res. 2022;50:W345–51.

Figures

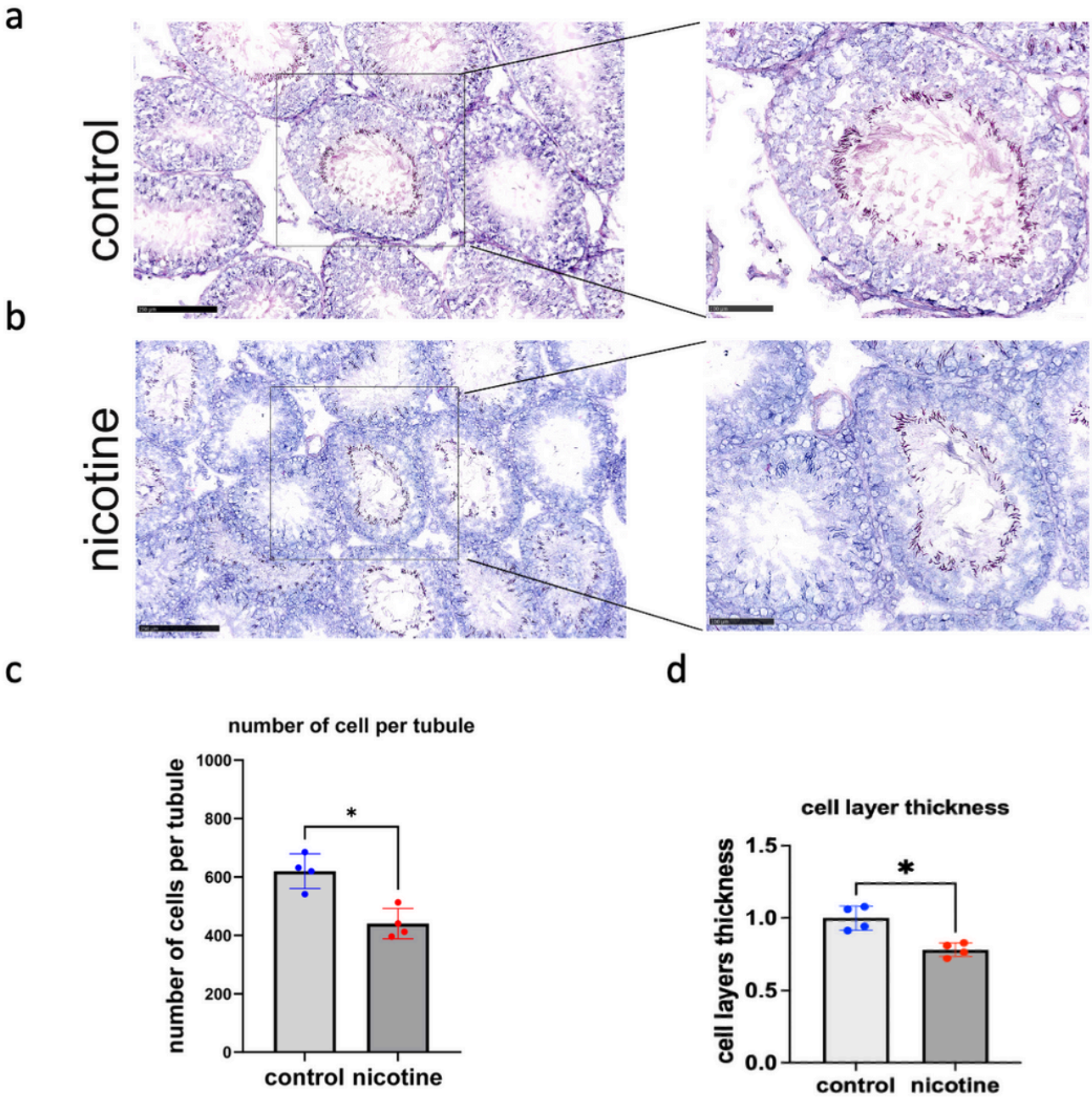

Figure 1

Testis morphology in Sprague-Dawley male rats prenatally exposed to nicotine. (**a**) Representative images of testes from mice derived from treatment doses of 0 and (**b**) 6 mg/kg/day of nicotine. The scale bars are 250 μM (left panels) and 100 μM (right panels). (**c**) Number of cells per tubule. (**d**) The thickness of seminiferous tubules, n=4 dose “0” and n=4 dose “6”; significance (*p<0.05) was determined by the Mann-Whitney test. All plots in the Figure represent averaged values +/-standard deviation. Rats were sacrificed at 11 weeks of age. The testes were flash-frozen, embedded in OCT and 7 mM frozen sections were stained with H&E. The photos were taken by using digital microscope nanozoomer and images were analysed. The cells were counted in stage (VI-VII) tubules.

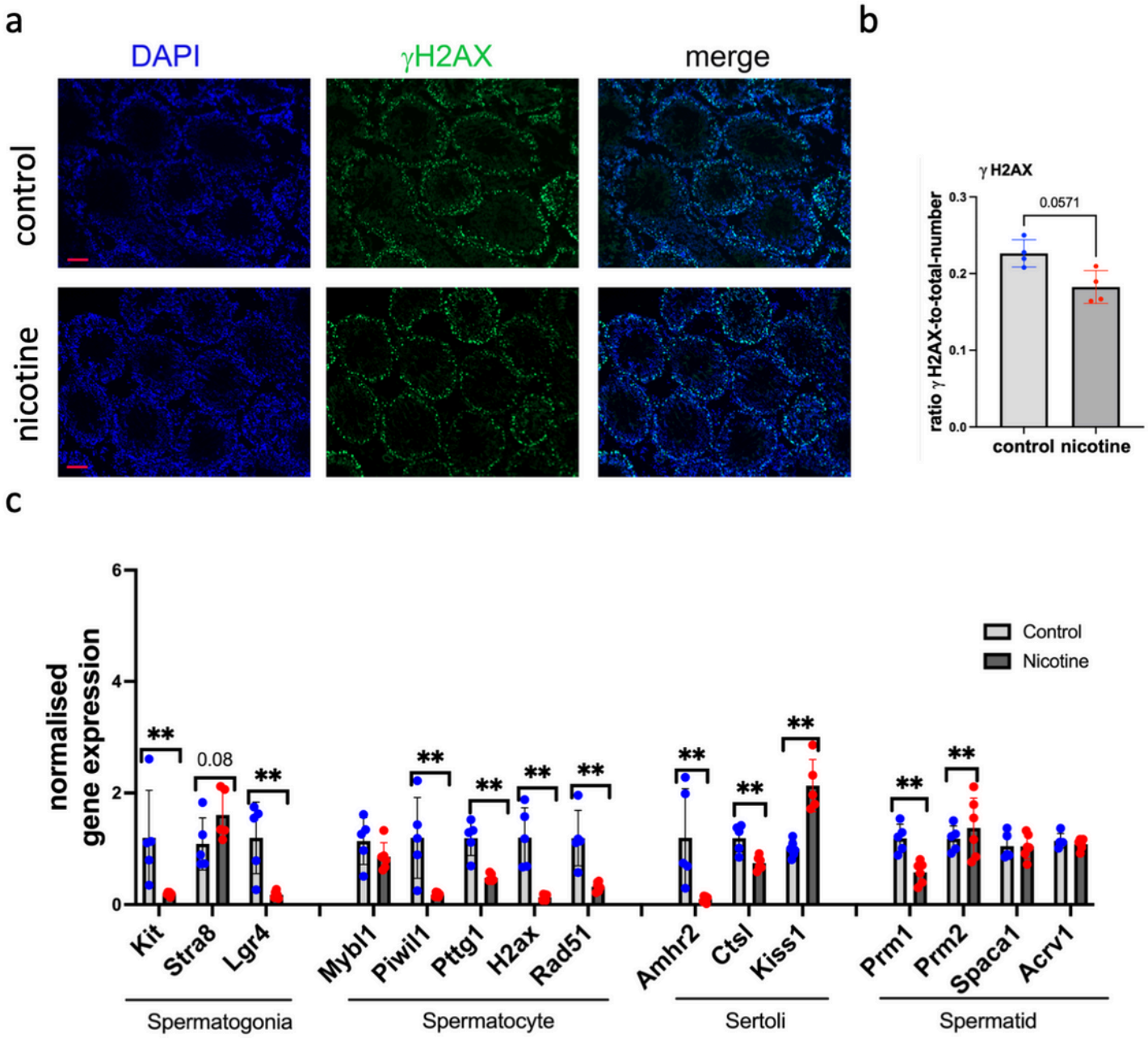

Figure 2

The effects of gestational nicotine exposure on meiotic and somatic testis cell. (**a**) Representative images of 11-week-old male testis spreads immunostained against gH2AX (green) in control (top) and nicotine (bottom) testis; the scale bar is 50 mM. (**b**) Quantitative analysis of a ratio of gH2AX-positive to total number of cells; n=4, dose “0”; n=5 dose “6, p-value is indicated on the top of the graph, non-parametric Mann-Whitney test. (**c**) The analysis of gene expression in 11-week-old testis by RT-qPCR; n=5

dose “0”; n=6 dose “6”. non-parametric Mann-Whitney test. All plots in the Figure represent averaged values +/-standard deviation.

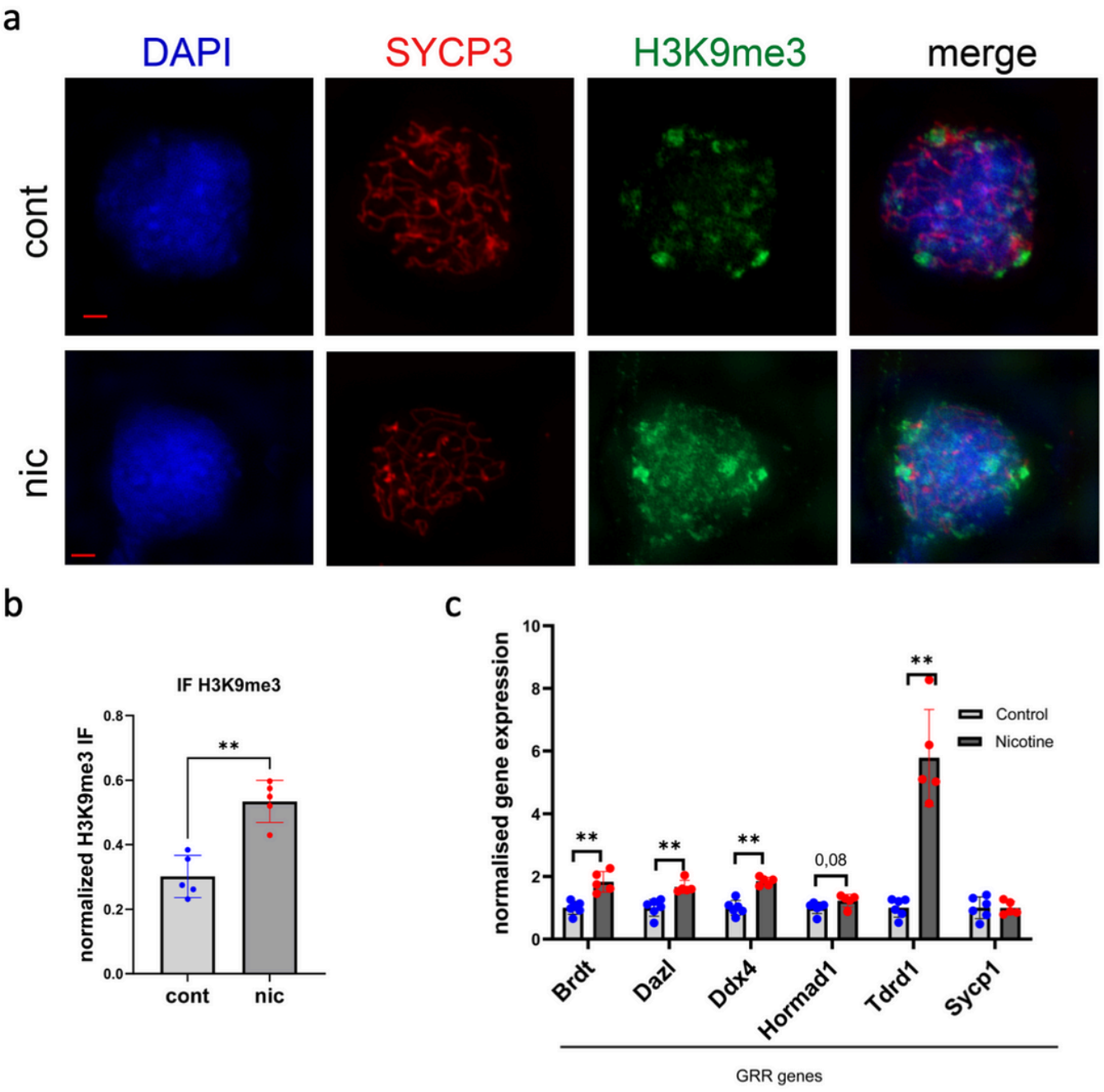

Figure 3

The effect of gestational nicotine exposure on H3K9me3 levels and GRRs gene expression. (**a**) Representative images of 11-week-old male testis spreads immunostained against H3K9me3 (red) or SYCP3 (green) in control (top) and nicotine-exposed mice; the scale bar is 5 μM. (**b**) Quantitative analysis of H3K9me3 staining intensity; n=5, dose “0”; n=5, dose “6, **p<0.01, non-parametric Mann-Whitney test.

(**c**) Quantitative analysis of GRRs gene expression in testis at 11-week-old males, n=6, dose “0”; n=5, dose “6”, **p<0.01, non-parametric Mann-Whitney test. All plots in the Figure represent averaged values +/-standard deviation.

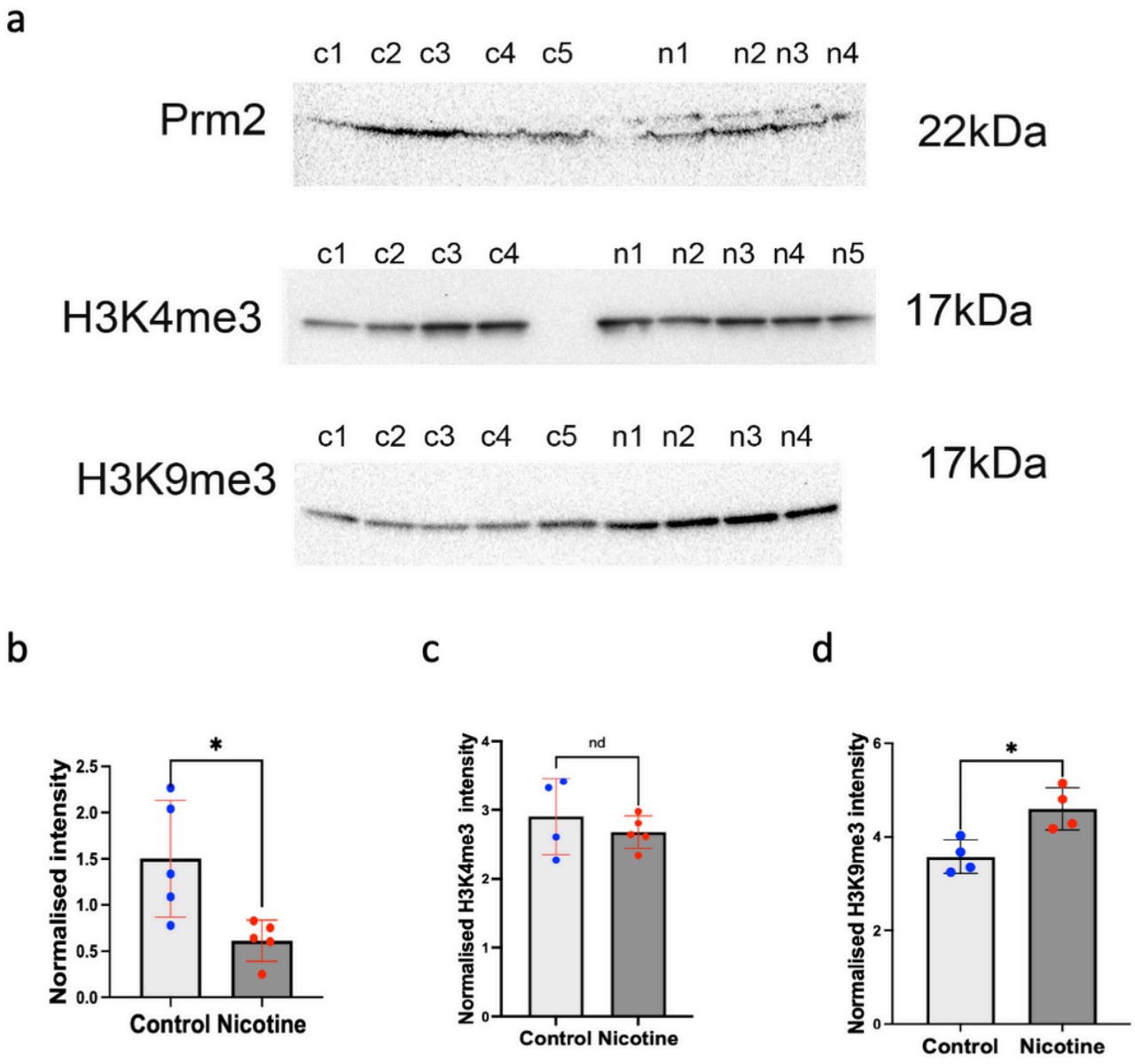

Figure 4

The analysis of protamine and histone expression in testis of control and nicotine-exposed rats. (**a**) Representative images of protamine PRM2 (top), H3K4me3 (middle) and H3K9me3 (bottom) Western blots of testis tissue; c1-c4 and c5 are controls and n1-n5 are nicotine-exposed samples. Quantitative

analysis of PRM2 (**b**), H3K4me3 (**c**), and H3K9me3 (D); n=4, (H3K4me3) or n=5 (H3K4me3, H3K9me3), control; n=4, (PRM2, H3K9me3), n=5 nicotine (H3K4m3) , *p<0.05 non-parametric Mann-Whitney test.

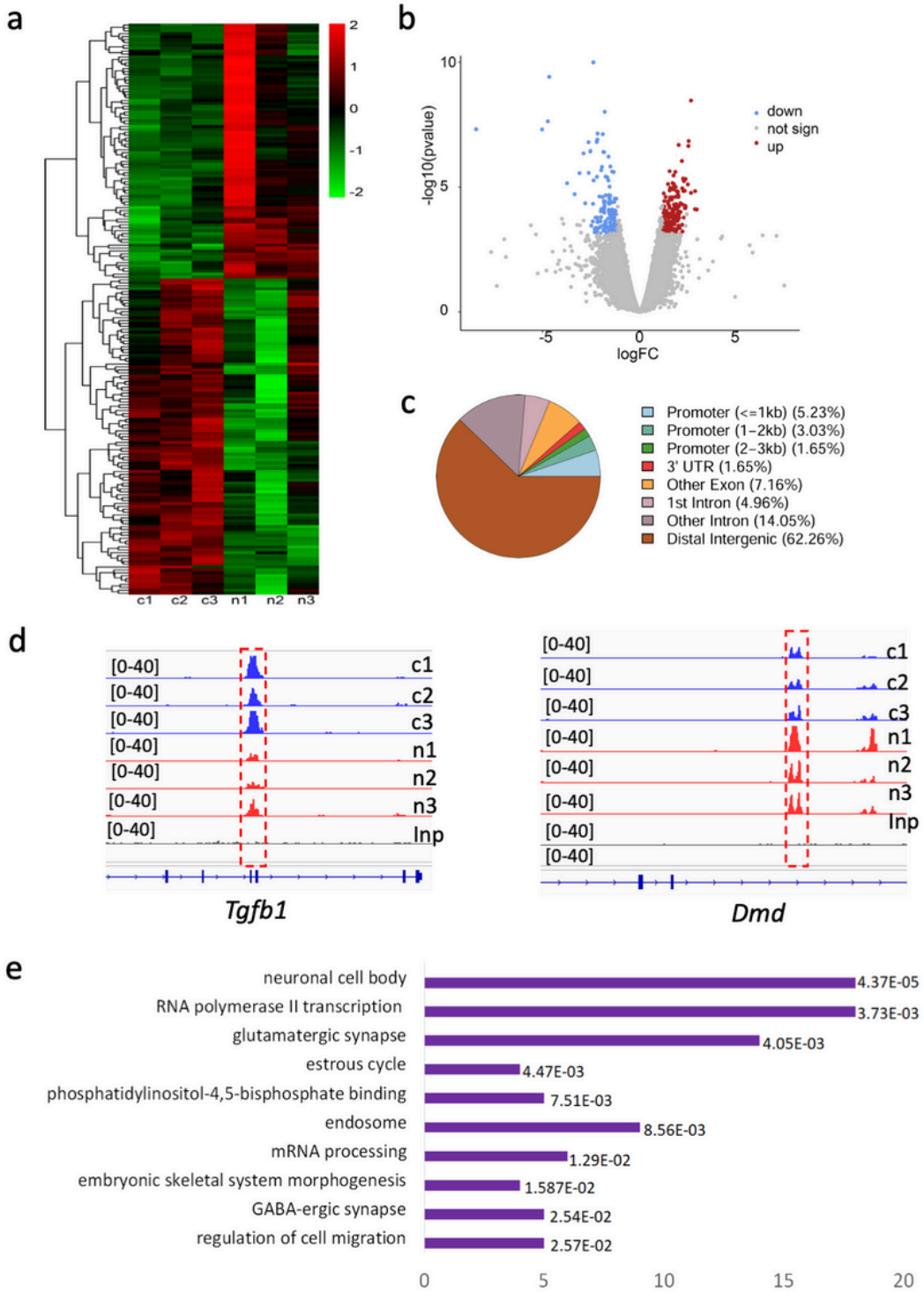

Figure 5

Genome-wide DNA methylation analysis of the 11-week-old rat testis. (**a**) A heatmap of all annotated DMRs. Counts were log transformed and plotted in R. (**b**) Volcano plot of DMRs. (**c**) Genomic localization of DMRs. (**d**) The differentially methylated peaks near *Tgfb1* and *Dmd* are shown in red dashed boxes.

Plots from control (*blue*) and nicotine-exposed (*red*) samples are shown. Each control and treatment group contained three replicates. The sequencing reads were mapped to the reference rn7 *Rattus norvegicus* genome, normalized and converted to bedgraph files, which were visualized in IGV. The signal intensity is shown in brackets. (**e**) Functional annotation as “biological process”, “cellular localization” or “molecular function’ of genes located in common DMRs by DAVID. Bars were sorted by adjusted p-values and the length of each bar represents the number of genes in this group.

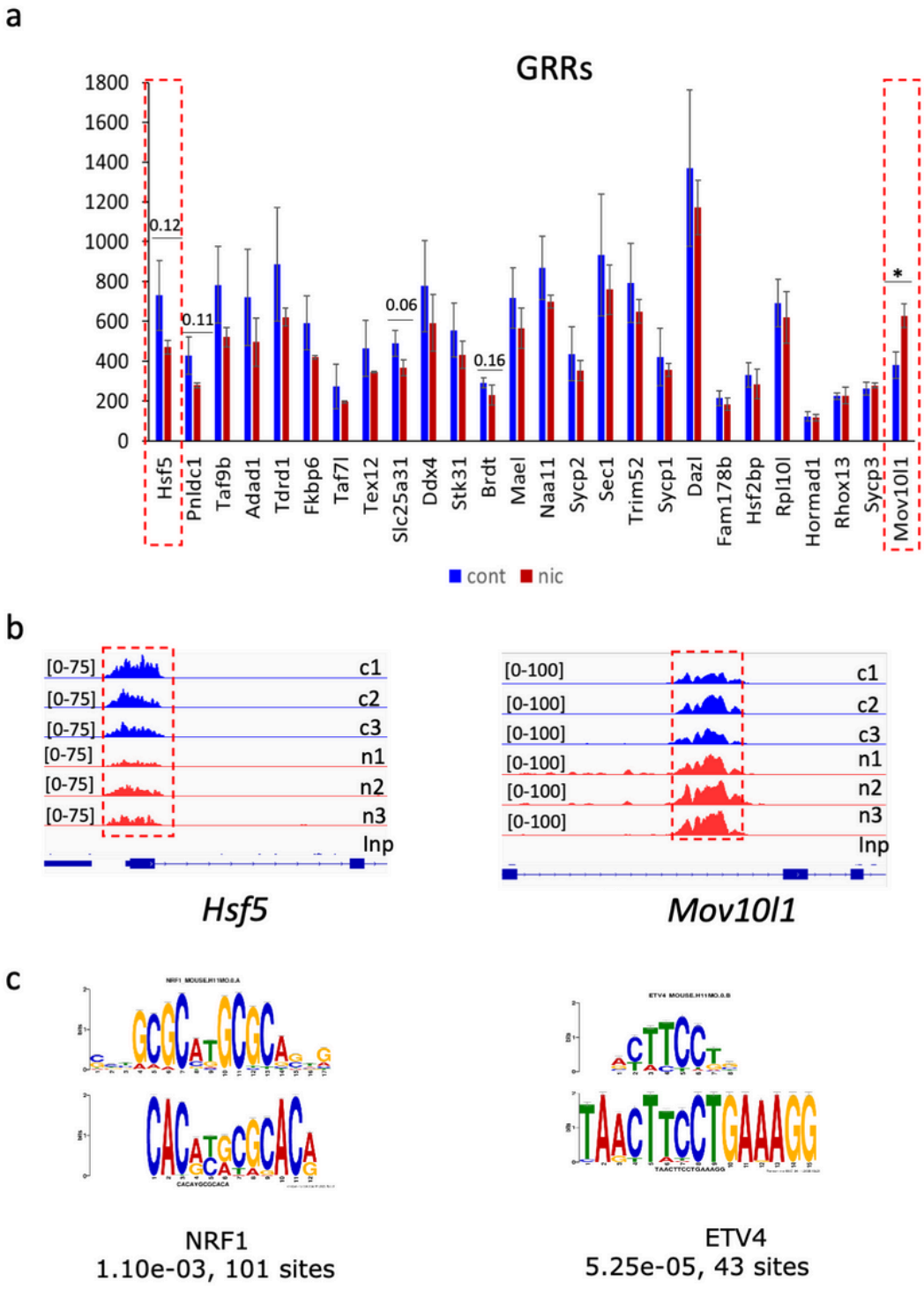

Figure 6

DNA methylation analysis of GRRs. (**a**) A plot of GRRs. Counts were extracted from sequencing data and plotted in Excel. (**b**) The differentially methylated peaks near *Hsf5* and *Mov10l1* are shown in red dashed boxes. Plots from control samples are shown in blue, plots from nicotine-exposed samples are shown in red. Each control and treatment groups contained three replicates. The sequencing reads were mapped to the reference rn7 *Rattus norvegicus* genome, normalized and converted to bedgraph files which were visualized in IGV, the signal intensity is shown in brackets. (**c**) Motif analysis by MEME-Chip revealed two enriched motifs, parts of these motifs are significant similar to NRF1 and ETV4 binding sites.

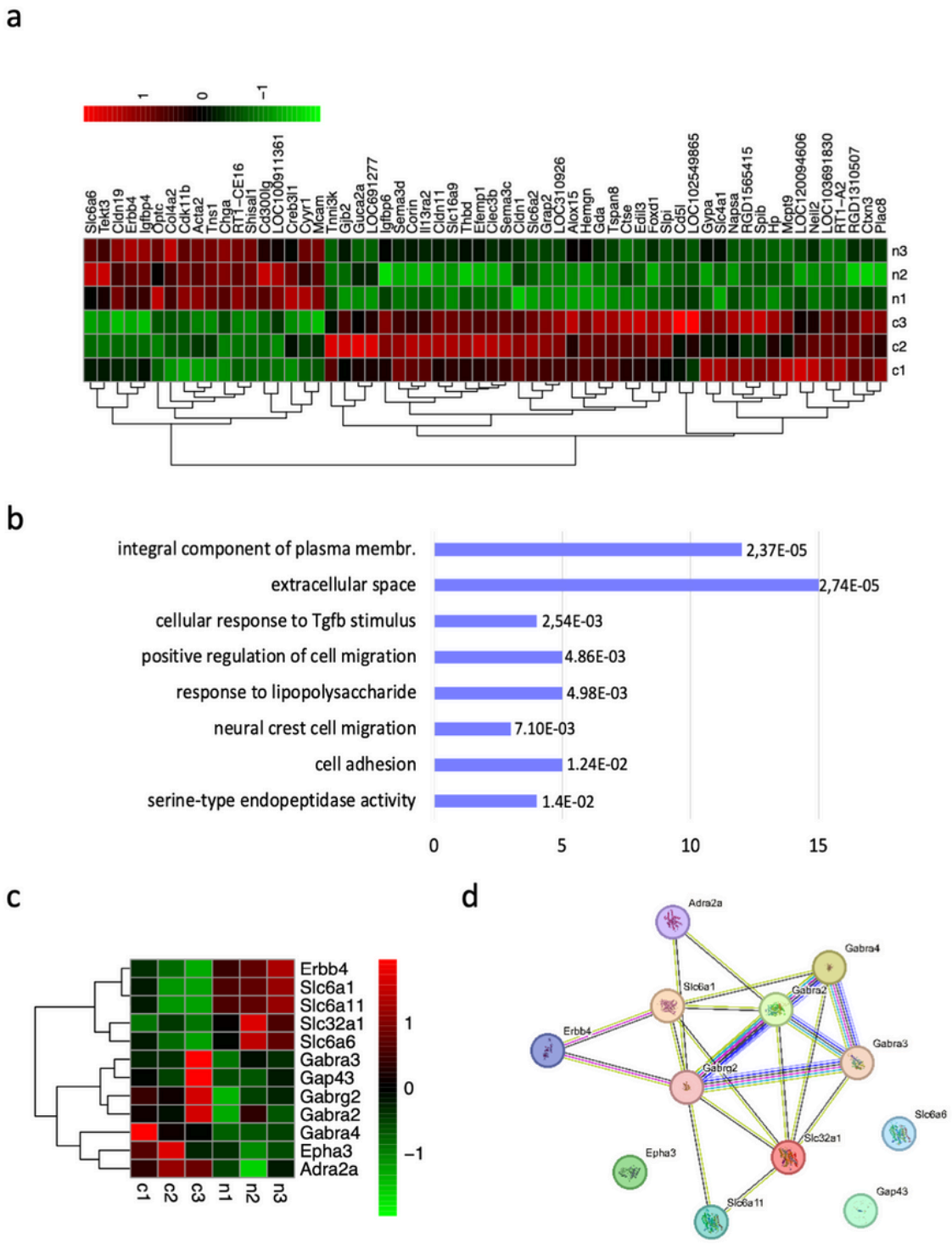

Figure 7

RNA-seq analysis in pituitary gland. (**a**) A heatmap of all annotated DMRs. Normalised counts were log transformed and plotted in R, c1-c3 control, n1-n3 nicotine exposed samples, upregulated genes are in red, downregulated genes in green. (b) Functional annotation “biological process”, “cellular component” or “molecular function” of DEG genes by DAVID, bars sorted by p-values, and each bar represents the number of genes in each group. (**c**) A heatmap of GABAergic signalling genes. The normalised counts were log transformed and plotted in R. (**d**) The network of GABAergic signalling genes, red line - indicates the presence of fusion evidence, green line - neighbourhood evidence, blue line - cooccurrence evidence, purple line - experimental evidence, black line - coexpression evidence, network was built by String (https://string-db.org/cgi/).

Supplementary Files

This is a list of supplementary files associated with this preprint. Click to download.

- Additionalfile1.xlsx
- Additionalfile2.xlsx
- MurielMurieletalsupplementary.pdf